RSC Advances

ROYAL SOCIETY
OF CHEMISTRY

www.rsc.org/advances

Journal Name

Dynamic Article Links ▶

ARTICLE TYPE

FRET-reporter nanoparticles to monitor redox-induced intracellular delivery of active compounds

Tina Gulin-Sarfraz,[a] Jawad Sarfraz,[a‡] Didem Şen Karaman,[a‡] Jixi Zhang,[a‡] Christina Oetken-Lindholm,[b] Alain Duchanoy,[a] Jessica M. Rosenholm[a*] and Daniel Abankwa[b*]

Nanoparticle-mediated drug delivery holds great promise for more specific and efficient therapies, mostly due to their high payload and the integration of targeted delivery functions. However, it is typically not possible to monitor the intracellular release of active compounds directly, which hampers the assessment of novel delivery platforms and non-cytotoxic compounds. Herein, we implemented a FRET ₁₀ (fluorescence resonance energy transfer)-reporter system to semi-quantitatively follow the time-course of the intracellular release of a redox-cleavable compound from a nanoparticle delivery platform. We used silica core-shell particles that could be readily modified with a high density of reactive amino groups, and attached fluorescent reporter molecules as model drug cargo. We coupled a FRET-donor fluorophore via a stable covalent bond, while the FRET-acceptor fluorophore was linked via a disulfide-bridge. ₁₅ Therefore, a loss of FRET reported on redox-induced acceptor compound release. These FRET-reporter nanoparticles allowed us to determine both the time course of cellular internalization as well as the intracellular compound release. Our data show that particle internalization is the rate-limiting step, while compound cleavage occurs fast after internalization. The presented FRET-reporter approach has the advantage to directly monitor the compound cleavage, as compared to indirect read-outs that are based on ₂₀ their cytotoxic action. We therefore propose that our FRET-reporter particles are suitable to monitor intracellularly redox-releasable compounds that are typically not cytotoxic, such as siRNAs.

Introduction

Silica nanoparticles have attracted much attention as ₂₅ biocompatible, biodegradable and flexible delivery platforms for biomedical applications.[1-7] The current focus in nanoparticle design is largely directed towards more complex structures with advanced drug delivery properties. One versatile design approach for obtaining such structures is the construction of core-shell ₃₀ particles, which integrate specific functionalities in a modular fashion. These nanoparticles consist of layers of two or more materials with distinct properties arising from the core and the shell layer, where especially the shell material is tailored towards the intended use of the particles.[8] To date, core-shell particles ₃₅ have successfully been applied within biomedical imaging, controlled drug release, targeted drug delivery, cell labeling, and tissue engineering.[8,9]

Coating of the core material can enhance the colloidal stability and dispersability, protect the core material, as well as simplify ₄₀ further functionalization of the particle system.[8] For instance, silica coating of inorganic nanoparticles can increase hydrophilicity and thus enhance dispersion of the particles in aqueous media,[10] which is critical for most biomedical applications. Moreover, as silica is optically transparent it is ₄₅ suitable for coating of optically active core materials such as quantum dots, where it also has the added benefit of enhancing the biocompatibility of the QDs.[11] Due to these attractive properties, inorganic cores coated with a silica shell have gained widespread use.[8,12-14]

₅₀ One of the most significant features of silica surfaces is to allow for straightforward surface functionalization, which enables tailoring of the surface charge and chemistry, as well as attachment of targeting ligands or other active moieties. Here, amino-functionalized surfaces are among the most common ₅₅ surface modifications especially for biomedical applications, since the most commonly applied strategies for bioconjugation of active molecules relies on amino-chemistry. Another important aspect for facilitating such modifications is to have a high surface density and stable anchoring of the reactive amino groups. A ₆₀ straightforward one-step procedure to realize this is by growing a hyperbranched poly(ethylene imine) (PEI) layer directly from the silica surface.[15-17] As the polymer is covalently grown from the hydroxyl groups on the silica surface, a high thermal and pH stability can be achieved.[18] In addition, the attained high positive ₆₅ particle surface charge and consequently, colloidal stability of the particle system, typically increase cellular uptake that can be initiated through electrostatic interactions with the negatively charged cell membrane of mammalian cells.[19-21]

Due to the layered multifunctionality that can be obtained via ₇₀ expedient surface modification, functionalized core-shell particles

RSC Advances Accepted Manuscript

are often used as delivery platforms for drugs or other biomedically relevant compounds. These cargos can either be covalently or non-covalently attached to the nanoparticles.[22] If the drug is non-covalently attached, the particles have either a stabilizing pocket for the drug or an encapsulating mechanism, where other molecules have to be cleaved from the surface in order to release the drug.[23,24] Controlled drug release is frequently desired and can be triggered by external or internal stimuli, such as light, a magnetic field, temperature, pH, hydrophobicity and biochemical reactions.[1,21] In the latter case, the covalent linkage of active compounds ideally utilize a cellular stimulus for its cleavage, such as the reducing environment inside a cell.[25] In order to exploit this, drugs can be covalently attached via disulfide bonds.[26-28] A disulfide bond is formed by oxidation of two sulfhydryl groups. Even though it is reversible it is relatively stable in blood plasma.[29] Formation of the disulfide bond is favored in the oxidizing extracellular space, while the bond is usually cleaved inside cells by molecules in the cytosol that carry sulfhydryl groups, such as glutathione.

Fluorescence methods have become one of the most important tools in bioscience, with fluorescence (or Förster) resonance energy transfer (FRET) being widely used for analyzing interactions of biological macromolecules, such as proteins, or to monitor signaling activities in living cells.[30,31] The FRET method allows to investigate molecular processes below the optical resolution limit of microscopes, as it exploits the non-radiative energy transfer from an excited donor molecule to an acceptor molecule; the efficiency of this process depends on distances of typically 1-10 nm.[32-34] FRET has been extensively used for bioaffinity assays,[35-37] studying nucleic acids,[38] multicolor imaging techniques,[39] biosensors,[40-47] or cleavage of covalent bonds by intracellular processes.[48,49]

Here, we follow the intracellular delivery of a compound that is attached to a polymer-modified silica core-shell nanoparticle, using FRET. A solid silica core was employed as an exemplary inorganic core that was coated with a porous silica shell, which considerably increased the available surface for ensuring efficient amino-functionalization. Redox-sensitive cleavage of a disulfide-linked FRET-fluorophore that acts as a reporter-compound, was followed and correlated with particle internalization into cancerous HeLa cells. With this approach, we were able to observe specific intracellular cleavage and particle internalization.

Results

Synthesis of PEI-functionalized core-shell nanoparticles as delivery platform

In order to have a flexible platform for nanoparticle-mediated delivery of bioactive compounds, we produced amino-functionalized core-shell particles with a solid silica core and a mesoporous silica shell. The porous coating was synthesized according to our previously published procedure,[50] which is suitable for the construction of large-pore shells on many types of inorganic solid cores, owing to the neutral synthesis conditions. Electron microscopy (EM) was used to determine the size, morphology and structure of the particles before and after coating. We obtained uniform, spherical cores (nSiO$_2$) of around 270 nm in diameter as determined by SEM (Fig. 1a). The size
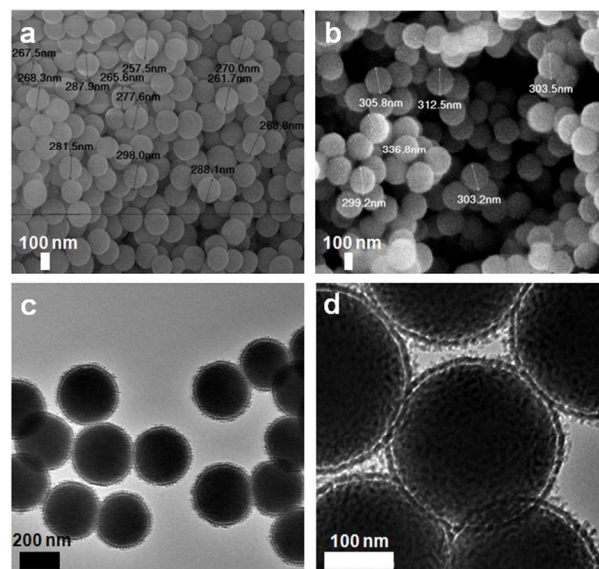
Fig.1 Electron microscopy of silica core-shell particles coated with a thin mesoporous layer. Electron microscopic images of nSiO$_2$ and nSiO$_2$@mSiO$_2$ particles. (a) SEM image of the silica core particles only (nSiO$_2$), and (b) the cores coated with the mesoporous silica shell (nSiO$_2$@mSiO$_2$). A scale bar of 100 nm is shown in the SEM-images, along with example diameters of the particles. (c) and (d) TEM images at two different magnifications revealing the structure of the silica shell (nSiO$_2$@mSiO$_2$). The images show scale bars of 100 nm and 200 nm, respectively.

increased to around 300 nm for the core-shell particles (nSiO$_2$@mSiO$_2$), due to the formation of a thin porous silica layer (Fig. 1b). TEM analysis confirmed that the structure of the coating was indeed porous (Fig. 1c,d). To further evaluate the pore size distribution and pore volume of the shell, nitrogen sorption was employed, using the density functional theory (DFT) for analysis.[51,52] The mesoporous silica shell had a pore size of 7 nm with a specific pore volume of 0.14 cm^3/g of the total particle mass (Fig. 2), which agrees with what would be expected from block-co-polymer templated mesopores.[53] The surface area was determined using the Brunauer-Emmett-Teller (BET) theory,[54] yielding a specific surface area of 62 m^2/g.

Next, we amino-functionalized the core-shell nanoparticles with a surface-grafted hyperbranched poly(ethylene imine) (PEI) layer, to ensure proper anchoring of the polymer to the surface throughout the subsequent functionalization steps. Electrokinetic measurements (zeta potential) as well as thermogravimetric analysis (TGA) confirmed successful PEI-functionalization. The ζ-potential measurements showed that the PEI-functionalized particles, nSiO$_2$@mSiO$_2$@PEI, obtained a high positive charge (+45 mV) upon surface modification, while the plain core-shell particles (nSiO$_2$@mSiO$_2$) exhibited a negative charge characteristic of its silica surface (-30 mV) (Supplementary Fig. S1). For comparison, the silica cores were PEI-functionalized directly (nSiO$_2$@PEI), which also resulted in a high positive ζ-potential (Table 1). While the core and core-shell particles displayed a similar net surface charge after PEI functionalization, TGA analysis revealed a ten-fold increase in the PEI-content of the nSiO$_2$@mSiO$_2$@PEI particles as compared to the nSiO$_2$@PEI particles (Supplementary Fig. S2). The PEI-content of the functionalized nSiO$_2$@mSiO$_2$ particles was 7.3 wt%, whereas
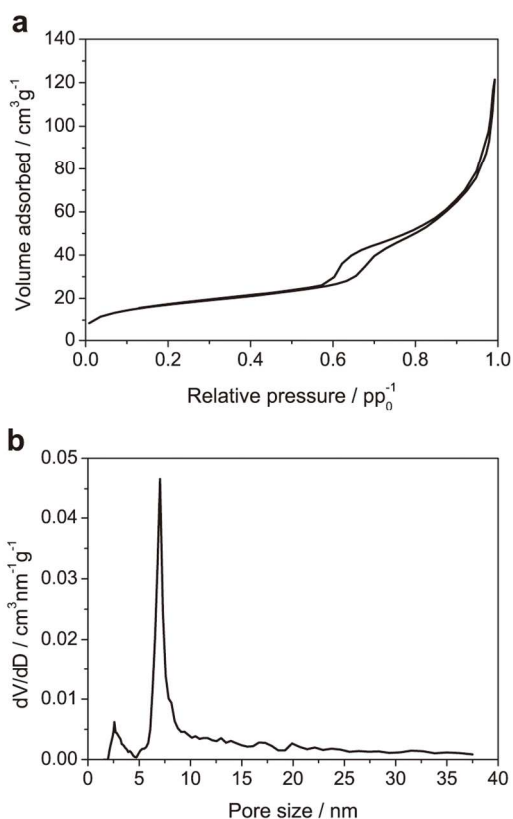
Fig.2 The coated silica layer is porous with pores of uniform size. Determination of structural characteristics of nSiO$_2$@mSiO$_2$ particles with nitrogen sorption. (a) Nitrogen sorption isotherm of nSiO$_2$@mSiO$_2$
5 particles. (b) Pore size distribution as determined by the DFT method. The peak at 7 nm corresponds to the average pore diameter.

Table 1 The effect of a thin porous coating on PEI functionalization efficiency. Electrokinetic measurements (zeta potential, Supplementary Fig. S1) and the mass loss determined with thermogravimetric analysis
35 (TGA, Supplementary Fig. S2) of the plain silica core-shell particles (nSiO2@mSiO2), PEI-functionalized silica cores (nSiO$_2$@PEI) and PEI-functionalized core-shell particles (nSiO$_2$@mSiO$_2$@PEI) are listed. Both of the PEI-functionalized particles obtained a high positive charge, while the thin porous silica coating significantly increased the efficiency of the
40 surface-grown PEI ten-fold.

Particle	Mass loss / %	Zeta pot. / mV
nSiO$_2$@mSiO$_2$	0.0	-30
nSiO$_2$@PEI	0.7	+44
nSiO$_2$@mSiO$_2$@PEI	7.3	+45
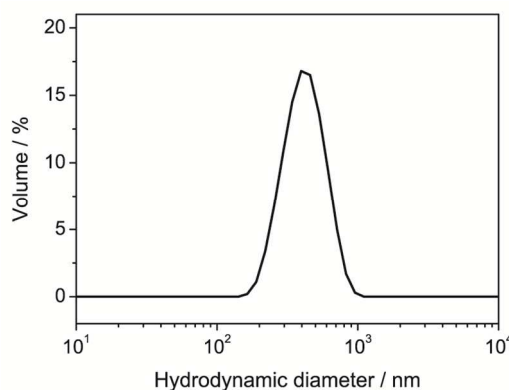
Fig. 3 The nSiO$_2$@mSiO$_2$@PEI particles are well dispersed in buffer
45 solution at physiological pH. Dynamic light scattering (DLS) of PEI-functionalized nSiO$_2$@mSiO$_2$ particles dispersed in HEPES buffer (25 mM, pH 7.2). Size distribution analysis from three measurements yields an average hydrodynamic diameter of 393 nm ± 6 nm (s.d.) for the particles.

without the porous shell the obtained PEI amount was merely 0.7 wt%.

10 We then determined the hydrodynamic size distribution of the nSiO$_2$@mSiO$_2$@PEI particles dispersed in HEPES buffer at physiological pH by dynamic light scattering (Fig. 3). The well-defined peak centered at 400 nm indicated that the functionalized particles were completely dispersible in aqueous solvent.

15 In summary, fully dispersible PEI-functionalized silica particles of core-shell type were obtained as prototypic compound delivery platform. Importantly, the thin porous silica coating significantly increased the available surface for amino-functionalization, which facilitates high density coupling of
20 active compounds without loss of favorable physico-chemical properties for aqueous conditions.

Development of a FRET-reporter system to detect release of surface-conjugated compounds

In order to measure the intracellular release of a reporter-
25 compound that is coupled to the surface amino-groups via a redox-cleavable thioether-linkage, one possibility could be to monitor the cleavage of a fluorophore. However, the initial fluorescence on the particle and released fluorescence would remain the same in total, precluding analysis by intensity
30 changes. Moreover, it is difficult to quantify the redistribution of fluorescence within the cell or even within the endocytic

50
vesicular compartments that contain the nanoparticles. We therefore developed a FRET-reporter system, where cleavage leads to a successive loss of FRET on the nanoparticles (Fig. 4). FRET is often used as a measure for the proximity between two
55 biomolecules that are labeled with a donor- and acceptor-fluorophore.[55] However, in order to establish a FRET-measure for compound release, we exploited the fact that on 2D-surfaces, such as on our particles, FRET depends on the fluorophore density and on the donor-acceptor ratio.[56]

60 We coupled the donor molecule, fluorescein isothyocyante (FITC), to the particle through a stable isothiocyanate bond to the amino-groups. Subsequently, sulfo-rhodamine (Rh-SH) was coupled to the particle surface through a redox-labile disulfide bond. This was introduced using SPDP (Succinimidyl-3-(2-
65 pyridyldithio)-propionic acid) as a linker between Rh-SH and the surface amino-groups (Fig. 4). We expected that the cleavage of the acceptor rhodamine would decrease the FRET signal, which would thus serve as a semi-quantitative measure for compound (in this case acceptor molecule) release.

70 In order to have highly fluorescent particles with densely conjugated fluorophores, we first established the highest surface concentration of FITC that does not lead to self-quenching. We followed the change of the fluorescence intensity of PEI-functionalized particles that were conjugated with FITC at
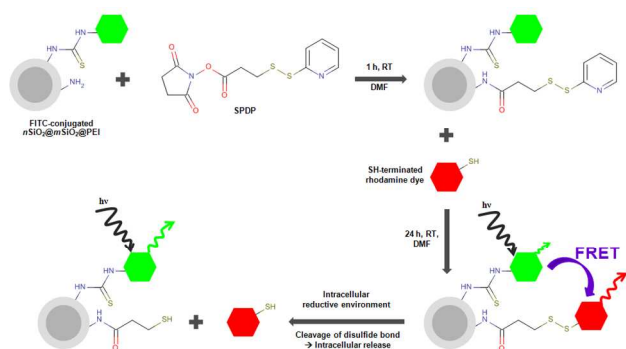
Fig.4 Schematic illustrations of the coupling procedure of the acceptor compound and the FRET approach. Schematic diagram of the FRET-reporter particle synthesis and redox-induced cleavage. The
5 FRET-donor fluorescein (as FITC) was stably coupled to the amino-functionalized nanoparticle, while the acceptor rhodamine (Rh-SH) was covalently linked via a redox-sensitive disulfide linker. The loss of FRET due to disulfide cleavage inside the cell is illustrated.

10 concentrations between 0.0001 wt% and 1 wt% FITC (Fig. 5). At concentrations above 0.1 wt% the fluorescence intensity did not increase further, but instead decreased, suggesting that significant self-quenching,[57,58] due to a too high density of FITC occurred. We therefore decided to fix the FITC concentration at 0.01 wt%,
15 which was one order of magnitude below the concentration that led to self-quenching.

Next, we established that a higher number of acceptor molecules as compared to donor molecules increased the FRET on the particles. We measured the fluorescence emission
20 spectrum of fluorophore-conjugated particles at different donor:acceptor ratios on a fluorescence spectrometer (Fig. 6). As expected, we observed a decrease in donor emission and increase in the acceptor emission as compared to the donor-only control, due to donor quenching and sensitized acceptor emission in
25 FRET. Decreasing the ratio of donor:acceptor on the particle, increased the donor quenching and sensitized acceptor emission and therefore FRET. The redox-induced cleavage of the acceptor-compound from the particle surface was first demonstrated under sink conditions by exposure to reducing agents at intracellular
30 concentration (Supplementary Fig. S3).

In order to image compound release in cells by FRET, we decided to use confocal microscopy. We first validated that we can detect FRET-level changes on the particles by microscopy. Therefore, we imaged particles with decreasing donor:acceptor
35 ratios and determined the FRET level as a FRET-ratio index. Increasing the amount of acceptor relative to the donor up to 10-fold increased the FRET successively (Fig. 7). In order to have a high starting FRET-level and thus better dynamic range for detecting compound cleavage, we chose the particles with the
40 highest donor:acceptor ratio of 1:10 for subsequent experiments in cells.

Intracellular cleavage of a nanoparticle-conjugated compound

With these high-FRET reporter-particles, we were now equipped
45 to determine the internalization of particles and intracellular compound release. In order to determine the time-course of cellular uptake of the particles, we used flow cytometry. HeLa
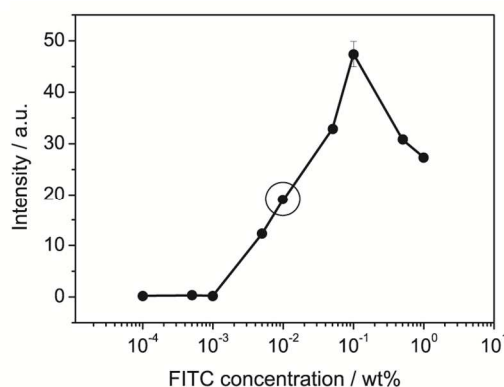
Fig. 5 Optimization of the donor concentration on the
50 **nSiO$_2$@mSiO$_2$@PEI particles.** The fluorescence intensity (excitation at 488 nm, emission at 518 nm) of nSiO$_2$@mSiO$_2$@PEI particles labelled with different concentrations (wt%) of FITC was measured in order to determine the FITC concentration for final fluorescence labelling. The graph shows an average of two measurements with standard deviations.
55 When the particles are conjugated with a very high concentration of FITC, the intensity drops due to self-quenching. The circle represents the donor-concentration chosen for labeling of the nSiO$_2$@mSiO$_2$@PEI starting material for the subsequent FRET-reporter particle preparation.
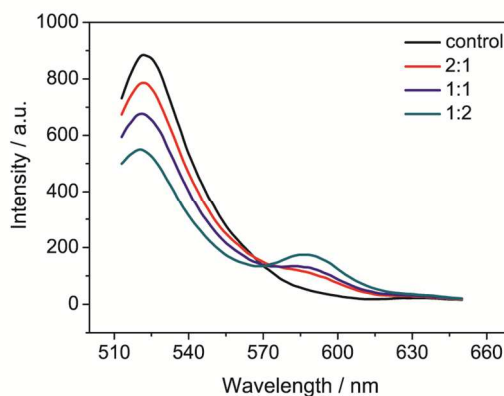
60 **Fig. 6 FRET increases with increasing relative acceptor concentration.** FITC-labelled nSiO$_2$@mSiO$_2$@PEI particles were further conjugated with different concentrations of the acceptor, Rh-SH, and the fluorescence intensity of the particles was measured between 510 and 650 nm, using 488 nm excitation. The ratios donor (FITC):acceptor (Rh-SH)
65 varied between 2:1 – 1:2. Particles labelled only with FITC were used as a non-FRET control. When increasing the donor:acceptor ratio on the particles, a decrease in the emission peak for the donor (520 nm) and an increase in emission for the acceptor (590 nm) were observed, indicating FRET.

70

(human cervical cancer) cells were incubated with particles and after various internalization times analyzed by flow cytometry. In order to detect only internalized particles, the extracellular fluorescence was quenched with trypan blue. Already after 1 h of
75 incubation basically all of the cells had internalized particles, as indicated by a complete peak shift (Fig. 8). This observation indicates an efficient and steady particle internalization process, which 24 h after incubation shifted the intensity histogram maximum approximately 4-fold.

80 We then moved on to image intracellular cleavage by FRET after particle uptake. HeLa cells were incubated with the FRET-particles under normal culture conditions (Fig. 9) and then fixed with formaldehyde after different internalization times.

a

b

c
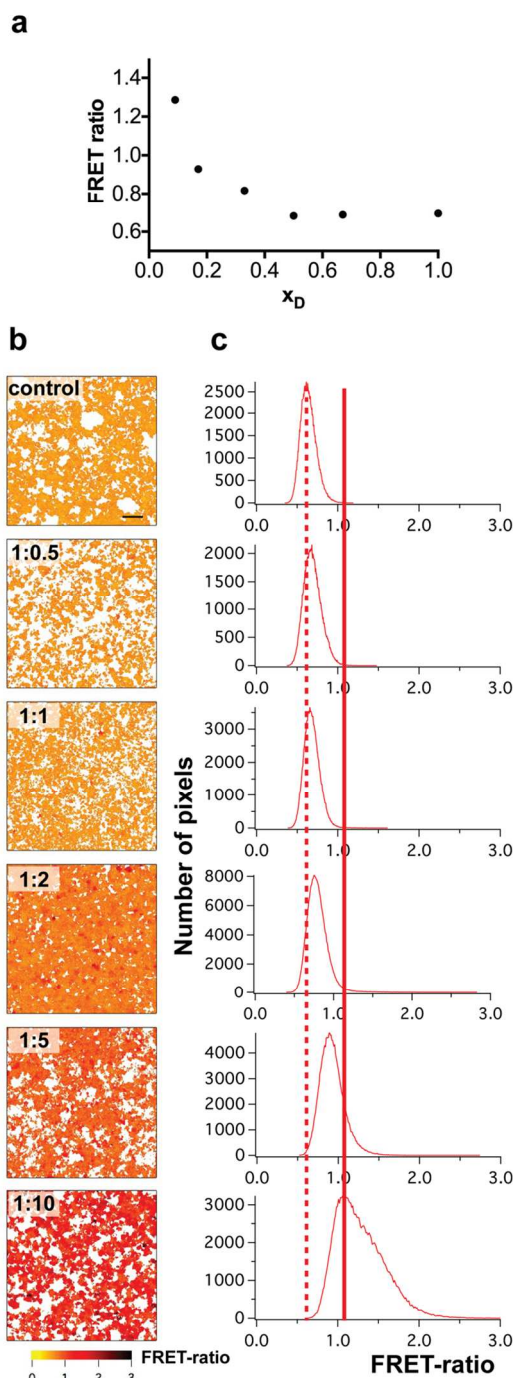
Fig. 7 Optimization of the FRET reporter by increasing the donor:acceptor ratio on the nSiO$_2$@mSiO$_2$@PEI particles. (a) FRET increases with smaller donor mole fraction (xD) on the particles. The
5 FRET-ratio was calculated as the average pixel-value from images shown in (b). The donor mole fraction (xD) was calculated from the wt%-ratios that were used in the conjugation reactions and that are shown in the labels of (b). (b) Confocal images of silica particles labeled with donor (FITC) and acceptor (Rhodamine)-fluorophores at the indicated
10 donor:acceptor ratios. The control sample is a 1:1 mix of silica particles loaded with donor- and acceptor-only. The look-up table shows the FRET-ratio color-coded with high FRET levels in black and low FRET in yellow. (c) Histograms of the pixel FRET-ratio of corresponding images shown to the left in (b). The dotted vertical line indicates the control
15 FRET-ratio level, while the solid line marks the high FRET maximum of the histogram of the sample with highest relative acceptor-concentration. Data are representative of two repeats.
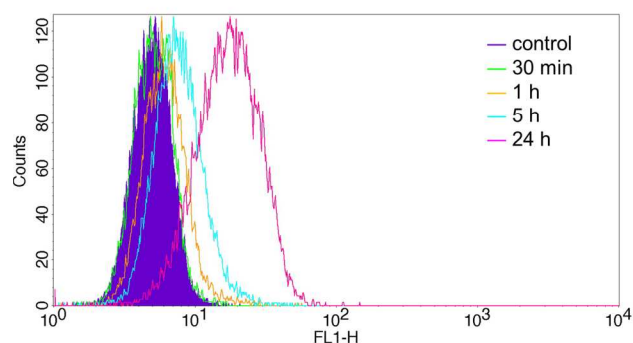
Fig. 8 Cellular uptake of FITC-labelled nSiO$_2$@mSiO$_2$@PEI
20 particles. The uptake of FITC-labelled nSiO$_2$@mSiO$_2$@PEI particles in HeLa cells was studied by flow cytometry at a particle concentration of 20 µg/ml. The shaded area is the control without particles. Increasing fluorescent particle uptake by the cells is seen by higher fluorescence intensity values in the FL1-H channel.

25 Correlation of cytometric internalization data and confocal FRET imaging data of these cells revealed that concomitant with particle internalization, the FRET-level within cells decreased, consistent with uptake induced cleavage of the model compound (Fig. 10). By contrast, particles with a non-cleavable FRET-pair
30 did not show changes in the FRET even after 24 h (Supplementary Fig. S4). A comparison of the particle-internalization and compound–cleavage time-courses showed that internalization depended linearly on the incubation time after the first hour, while cleavage from internalized particles occurred
35 much faster with an estimated half-time of less than 5 h (Fig. 10). Therefore, particle uptake into the cells is the rate-limiting process in compound delivery for this type of system. However, our data also suggest that a cellular response could already be expected at time points around the cleavage half-time, since the
40 observed cleavage is most pronounced within the first hour.

Discussion

We have successfully produced amino-functionalized core-shell nanoparticles with a covalently linked compound that is released inside a human cancer cell line due to redox-switching. A solid
45 silica particle of Stöber type was used as a core, representative of any inorganic colloidal material. The mesoporous silica shell served as a functionalization platform for growing high-density PEI surface functions. We established a FRET-reporter system, where the donor fluorophore was stably coupled to the amino-
50 groups, while the acceptor fluorophore was introduced as a redox-releasable compound via a thioether linkage. This enabled us to detect a fast redox-dependent cargo-compound release upon cellular uptake of the particles.

The coating was synthesized according to our previously
55 published mild procedure for large-pore mesoporous coating of magnetite beads under neutral conditions.[50] This will in the future allow for particle design that involves more diverse inorganic core materials, as it avoids high or low pH synthesis conditions that could lead to dissolution of the core. The porous shell
60 obtained via this route is characterized by mesopores larger than the "standard" size (3-4 nm) and is consequently more suitable for accommodating biomolecular cargo. In the present case, the porous layer allowed for efficient organic modification by surface hyperbranching polymerization of PEI. Surfaces coated with this
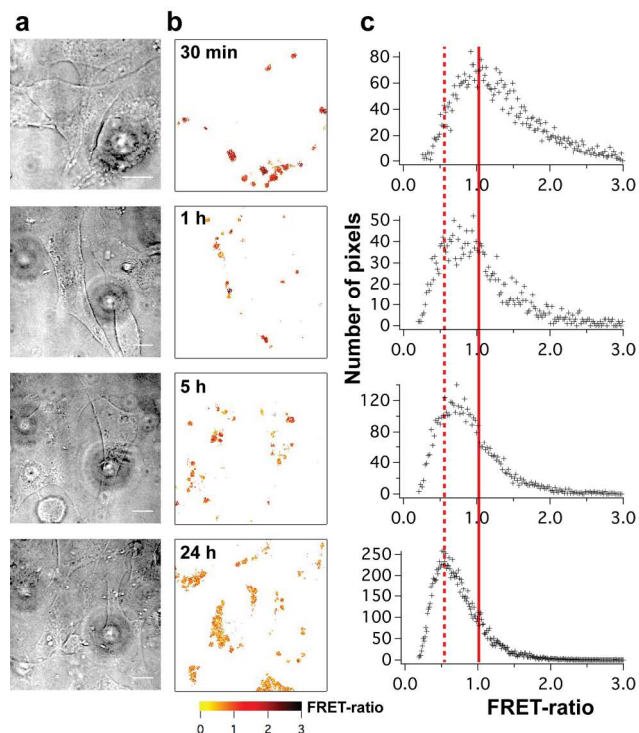
Fig. 9 Loss of FRET from silica particles after uptake into HeLa cells.
(a) Column of bright field images of cells incubated with silica-particles
that were labeled with donor:acceptor at 1:10 ratio. (b) FRET images of
5 cells shown in (a) with FRET-level on silica particles color coded from
yellow (low) to black (high). Incubation time of cells with particles is
shown. (c) Histograms of FRET-ratio per pixel of adjacent images shown
in (b). Scale bars in (a) are also representative for (b) and are 10 µm.

10 type of hyperbranched PEI possess a much higher amount of
amino-groups as compared to surfaces amino-functionalized
through conventional routes.[17] The high amount of primary
amino groups on the surface provide a high positive charge over a
wide pH-range (up to pH~11), which enhances the aqueous
15 dispersability of the silica particles as well as aids in keeping the
dispersion stable through electrostatic forces.[59] These particular
physiochemical properties, positive surface charge and high
colloidal stability of nanoparticles, are highly beneficial for
cellular uptake. It has also been demonstrated that PEI
20 modification of core-shell particles slows down the degradation
process of the silica shell, especially so for porous shells which
are more susceptible to hydrolytic degradation due to their
exposed nature.[60]

Intracellular release mechanisms are especially challenging to
25 study, albeit highly desired since drug release mechanisms
determined under sink conditions rarely present significant
relevance or correlation to actual biological or physiological
conditions. Consequently, the "release" of active compounds is
typically measured indirectly, often by determining the viability
30 of the treated cells. This greatly limits the assessment of the
biological effect of non-cytotoxic cargo. Additionally, such an
evaluation does not reveal how soon after internalization of the
nanocarrier the cargo itself is released, an information that is
relevant if more subtle cellular activity of cargo (such as e.g.
35 effect of siRNA) needs to be evaluated. Fluorescence-based
techniques enable quantitative or semi-quantitative
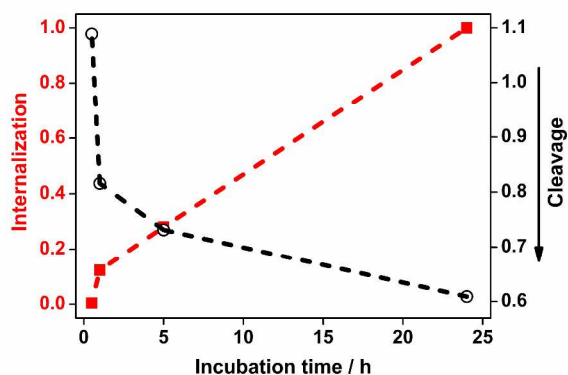
Fig. 10 Kinetics of particle uptake and acceptor compound cleavage.
The normalized intensity values of the positive cell population peaks in
40 Fig. 8 were plotted against the particle incubation time to illustrate the
time-course of internalization (red). In order to facilitate the correlation
between internalization and compound cleavage, the FRET-ratio values of
the histogram peaks in Fig. 9c (determined by Gaussian fitting) are
plotted on the same time axis, and they indicate the amount of uncleaved
45 acceptor.

measurements, and we developed a system that is tailored
towards semi-quantitative monitoring of compound release,
rather than assessing a particular cellular response to a particular
50 compound. Our FRET-reporter system allowed for the direct
observation of cargo-fluorophore cleavage. In some cases, it
should be possible to develop the system such that the reporter-
fluorophores are coupled to the actual bioactive cargo, which
would allow to directly and specifically follow internalization and
55 cleavage of such a cargo. Alternatively, a FRET-reporter system
could be linked to a delivery platform in the background, and
help to monitor the release of a compound that is coupled with a
similar release mechanism as the releasable FRET-fluorophore
(here the acceptor). In both cases, tracking of the internalization
60 path with fluorescent cell organelle markers and in parallel of the
FRET-signal can in the future help to address subcellular delivery
specificity of nanoparticles. Our results show that particle uptake
into the cells is highly efficient and that intracellular redox-
mediated cleavage occurs within a few hours after internalization.

65 # Experimental

Reagents and materials

Aziridine (98%) was purchased from Menadiona. Tetraethyl
orthosilicate (TEOS, ≥ 98%) and toluene (99.8%) were obtained
from Fluka. 3-[2-pyridyldithio]-propionic acid N-
70 hydroxysuccinimide ester (SPDP, ≥ 95%), N,N-
Diisopropylethylamine (DIPEA, 99.5%), N,N-
Dimethylformamide (DMF, ≥ 99.9%), Ammonium hydroxide
(NH3, 33 wt%), Trypan Blue, as well as sodium bicarbonate and
sodium carbonate used for the carbonate buffer, were purchased
75 from Sigma-Aldrich. Sodium chloride (NaCl, 99.7%) was
obtained from J. T. Baker and absolute ethanol (99%) from Altia.
Fluorescein isothiocyanate (FITC, 90%) and poly(ethylene
glycol)-block-poly(propylene glycol)-block-poly(ethylene glycol)
(P123) were obtained from Aldrich. Acetone (≥ 99.8%) and

acetic acid (CH$_3$COOH, $\geq$ 99.8%) were purchased from Merck. Sulforhodamineamidoethylmercaptan (sulfo-rhodamine, Rh-SH) was from Toronto Research Chemicals Inc. All chemicals used for the study were of analytical grade and milli-Q water (18.2 MΩ cm) was used throughout the study.

Synthesis of silica core-shell nanoparticles, nSiO$_2$@mSiO$_2$

The non-porous silica cores were synthesized by the Stöber method.[61] 100 ml ethanol, 15 ml milli-Q water and 1.45 ml NH3 were mixed by stirring. 7 ml TEOS were added and the solution was stirred at 500 rpm at room temperature for 24 h. The obtained particles were centrifuged at 9000 rpm for 15 min, washed with ethanol and acetone and finally dried in a vacuum oven for one day. The large-pore coating described by Rosenholm et al.[50] was used with slight modifications. 0.1 g P123 and 1.16 g NaCl were dissolved in 80 ml milli-Q water and 32 ml ethanol by using an ultrasonication bath for 15 min. 0.3 g silica cores were added and the solution was left for stirring at 300 rpm at 35 ˚C for 30 min. 0.45 ml TEOS was added and the stirring continued for 24 h. The template was extracted from the shell by sonication with acetone 3 times for 30 min.

Amino-functionalization and fluorophore-conjugation to the particles

0.2 g core-shell silica particles were vacuum-dried at 45 ˚C for 4 h after which they were dispersed in toluene under inert atmosphere. 100 µl aziridine and 10 µl acetic acid were added and the reaction mixture was stirred at 75 ˚C for 24 h. The particles were separated by centrifugation at 7500 rpm 10 min, washed by acetone and finally vacuum-dried. For fluorophore coupling, 10 mg PEI-functionalized particles were suspended in 1.5 ml carbonate buffer (pH 9) and fluorescein isothiocyanate (FITC) dissolved in DMF (1 mg ml^{-1}) was added at different amounts, ranging from 0.0001 wt% up to 1 wt%, depending on the intended FITC surface concentration. The reaction continued for 1 h after which the particles were separated by centrifugation and washed with water and acetone. The FITC-labeled particles were dried in vacuum. Next, sulforhodamineamido-ethylmercaptan (sulfo-rhodamine, Rh-SH) was coupled to the FITC-labeled particles through a cleavable disulfide bridge from succinimidyl 3-[2-pyridyldithio]-propionate (SPDP).[62] 10 mg particles were dispersed in 1.5 ml DMF. 10 µl DIPEA was added and the mixture was left to react for a 5 min. SPDP (1.0 mg ml^{-1} in DMF) was added and the mix was stirred for 1 h. Afterwards sulfo-rhodamine (1.0 mg ml^{-1} in DMF) was added and the stirring continued for 24 h. The molar ratio between SPDP and sulfo-rhodamine was kept constant, however, their total amount was varied as compared to the FITC amount in order to finally achieve different donor:acceptor coupling ratios. The particles were finally separated by centrifugation and washed with DMF and ethanol, and dried in vacuum.

Nanoparticle characterization methods

The morphology and size distribution of the nanoparticles were determined by scanning electron microscope using a Zeiss DSM 962 at 20 kV and a transmission electron microscope, JEOL JEM-2010 at 120 kV. The pore size distribution and surface area of the core-shell particles were measured by nitrogen sorption (Autosorb 1, Quantachrome) at 77 K. Thermogravimetric analysis (TGA-Netzsch STA 449F1 Jupiter) was used to determine the amount of organics added in the functionalization step. The mass loss was measured up to 1000 °C. Zeta potential measurements were carried out to determine the net surface charge of the core-shell particles before and after PEI-functionalization. Dynamic Light Scattering, DLS, was used for measuring the dispersability of the particles. For zeta potential and DLS measurements the instrument Malvern Zetasizer Nano ZS was used. The intensity of the fluorescent samples was measured with a PerkinElmer LS50B luminescence spectrometer as well as with a Varioskan Flash plate reader. Particles with different ratios between the donor and the acceptor molecules were also studied by confocal microscopy (Zeiss LSM510) in order to choose the best candidate for the cellular uptake study.

Cellular uptake determination by flow cytometry

For the cellular nanoparticle uptake experiments HeLa cervical carcinoma cells were cultured on 12-well plates in Dulbecco's modified Eagle's medium (DMEM; Sigma) supplemented with 10% fetal bovine serum (PAA), 2 mM L-glutamine (Sigma), at 37 °C and in 5% CO$_2$. FITC-labeled particles were suspended in cell media at a concentration of 20 µg ml^{-1}, and sonicated for 15 min. The particle suspension was added to the cells and incubated for 30 min, 1 h, 5 h and 24 h. After incubation the cells were washed in phosphate buffered saline (PBS), detached by trypsinization and centrifuged down at 2000 rpm for 5 min. The extracellular fluorescence was quenched by resuspending the cells in trypan blue (200 µg ml^{-1}) and incubating them for 10 min in room temperature. After washing once with PBS the cells were resuspended in PBS and analyzed with a BD FacsCalibur flow cytometer. The mean fluorescence intensity (MFI) of the cells at FL-1 channel (ex 488 nm, em 530/30) was measured. The data was analyzed with BD CellQuest ProTM software. The control peak (no particles) was subtracted, whereafter the resulting fluorescence intensity (MFI) value was multiplied with the fraction of positive cells as representation for internalization.

Confocal FRET-imaging

For the intracellular FRET-imaging HeLa cells were grown on round cover slips (Menzel). The cells were incubated with high-FRET particles, labeled with FITC and sulfo-rhodamine using the same concentrations and time points as mentioned above. Uptake was stopped by washing off most non-internalized particles with PBS and fixing of the cells with 4% paraformaldehyde (PFA; Sigma) for 20 min at room temperature. After washing with PBS the cells were mounted on microscope slides (VWR) using Mowiol/Dabco (Sigma/Aldrich). The glass slides were left for 24 h drying in the dark at room temperature. A Zeiss LSM 510 confocal microscope equipped with a 63x/ 1.4 oil DIC immersion objective was used to record 12 bit 512x512 fluorescent images, using 1000 or 500 µm pinhole size in the frame mode with 4x averaging. Sensitized acceptor emission ratio-FRET images were acquired using the following settings of donor (ex 458 nm, 3% laser power, em 500-545 nm), and FRET (ex 458 nm, 3% laser power, em 560 LP) channels. Presence of the acceptor was verified using 543 nm excitation and detection with a 560 LP filter. Zeiss' lsm-format images were converted into the Tif-format using Fiji[63] and processed further to calculate the background-corrected FRETratio=I FRET-channel/I donor-

channel (I: corrected intensity in a pixel) as a measure for FRET on a pixel-by-pixel basis in a custom written procedure in IgorPro6 (Wavemetrics, Oregon). Histograms of the pixel-intensities from the FRET-ratio image were then compared.

Conclusion

A high-FRET reporter-particle system was developed and applied to determine the internalization and compound-release kinetics of a prospective intracellular delivery platform of active agents. The delivery platform is composed of a paradigmatic solid silica core, coated with a porous silica shell. These $nSiO_2@mSiO_2$ particles were subsequently modified by surface hyperbranching polymerization of poly(ethyleneimine) (PEI). This yielded well-dispersed nanoparticles with a high amount of terminal amino groups for further attachment of active molecules. We stably attached a FRET pair of fluorescein and a rhodamine dye, where the latter was coupled via a redox-cleavable linker. Using sensitized acceptor emission FRET methods, the intracellular cleavage of the rhodamine molecules was studied in relation to the particle internalization process. Our results suggest that the presented design could be employed as a reporter-system for intracellular drug release.

Acknowledgements

Notes and references

ᵃ Center for Functional Materials, Laboratory for Physical Chemistry, Åbo Akademi University, Porthansgatan 3, 20500 Turku, Finland. Fax: +358 (0)2 233 0228; Tel: +358 (0)2 215 4253; E-mail: jerosenh@abo.fi

ᵇ Turku Centre for Biotechnology, University of Turku and Åbo Akademi University, Tykistökatu 6B, 20520 Turku, Finland. Tel: +358 (0)2 333 6969; E-mail: daniel.abankwa@btk.fi

† Electronic Supplementary Information (ESI) available: [details of any supplementary information available should be included here]. See DOI: 10.1039/b000000x/

‡ These authors contributed equally to this work.

1   Z. Li, J. C. Barnes, A. Bosoy, J. F. Stoddart, and J. I. Zink, *Chem. Soc. Rev.*, 2012, **41**, 2590–2605.

2   S. Simovic, N. Ghouchi-Eskandar, A. M. Sinn, D. Losic, and C. A. Prestige, *Curr Drug Discov Technol*, 2011, **8**, 269–276.

3   M. Varna, *Journal of Biomaterials and Nanobiotechnology*, 2012, **3**, 269–279.

4   J. M. Rosenholm, A. Meinander, E. Peuhu, R. Niemi, J. E. Eriksson, C. Sahlgren, and M. Lindén, *ACS Nano*, 2008, **3**, 197–206.

5   J. M. Rosenholm, C. Sahlgren, and M. Lindén, *Nanoscale*, 2010, **2**, 1870–1883.

6   T. Asefa and Z. Tao, *Chem. Res. Toxicol.*, 2012, **25**, 2265–2284.

7   P. Yang, S. Gai, and J. Lin, *Chem. Soc. Rev.*, 2012, **41**, 3679–3698.

8   R. Ghosh Chaudhuri and S. Paria, *Chem. Rev.*, 2012, **112**, 2373–2433.

9   W. Schärtl, *Nanoscale*, 2010, **2**, 829–843.

10   A. Guerrero-Martínez, J. Pérez-Juste, and L. M. Liz-Marzán, *Advanced Materials*, 2010, **22**, 1182–1195.

11   N. Ma, A. F. Marshall, S. S. Gambhir, and J. Rao, *Small*, 2010, **6**, 1520–1528.

12   J. Zhang, X. Li, J. M. Rosenholm, and H. Gu, *J Colloid Interface Sci*, 2011, **361**, 16–24.

13   E. von Haartman, H. Jiang, A. A. Khomich, J. Zhang, S. A. Burikov, T. A. Dolenko, J. Ruokolainen, H. Gu, O. A. Shenderova, I. I. Vlasov, and J. M. Rosenholm, *J. Mater. Chem. B*, 2013, **1**, 2358–2366.

14   N. Prabhakar, T. Näreoja, E. von Haartman, D. Ş. Karaman, H. Jiang, S. Koho, T. A. Dolenko, P. E. Hänninen, D. I. Vlasov, V. G. Ralchenko, S. Hosomi, I. I. Vlasov, C. Sahlgren, and J. M. Rosenholm, *Nanoscale*, 2013, **5**, 3713–3722.

15   C. O. Kim, S. J. Cho, and J. W. Park, *Journal of Colloid and Interface Science*, 2003, **260**, 374–378.

16   J. M. Rosenholm, A. Penninkangas, and M. Lindén, *Chem. Commun.*, 2006, **37**, 3909–3911.

17   J. M. Rosenholm and M. Lindén, *Chem. Mater.*, 2007, **19**, 5023–5034.

18   M. Sakeye and J.-H. Smått, *Langmuir*, 2012, **28**, 16941–16950.

19   C. He, Y. Hu, L. Yin, C. Tang, and C. Yin, *Biomaterials*, 2010, **31**, 3657–3666.

20   B. Yu, Y. Zhang, W. Zheng, C. Fan, and T. Chen, *Inorg. Chem.*, 2012, **51**, 8956–8963.

21   Z. P. Xu, Q. H. Zeng, G. Q. Lu, and A. B. Yu, *Chemical Engineering Science*, 2006, **61**, 1027–1040.

22   T. L. Doane and C. Burda, *Chem Soc Rev*, 2012, **41**, 2885–2911.

23   M. W. Ambrogio, T. A. Pecorelli, K. Patel, N. M. Khashab, A. Trabolsi, H. A. Khatib, Y. Y. Botros, J. I. Zink, and J. F. Stoddart, *Org. Lett.*, 2010, **12**, 3304–3307.

24   R. Liu, X. Zhao, T. Wu, and P. Feng, *J. Am. Chem. Soc.*, 2008, **130**, 14418–14419.

25   C. K. Sen, *Biochem. Pharmacol.*, 1998, **55**, 1747–1758.

26   J.-S. Lee, J. J. Green, K. T. Love, J. Sunshine, R. Langer, and D. G. Anderson, *Nano Lett.*, 2009, **9**, 2402–2406.

27   J. Jung, A. Solanki, K. A. Memoli, K. Kamei, H. Kim, M. A. Drahl, L. J. Williams, H.-R. Tseng, and K. Lee, *Angew. Chem. Int. Ed. Engl.*, 2010, **49**, 103–107.

28   R. Mortera, J. Vivero-Escoto, I. I. Slowing, E. Garrone, B. Onida, and V. S.-Y. Lin, *Chem. Commun.*, 2009, **22**, 3219–3221.

29   G. Saito, J. A. Swanson, and K.-D. Lee, *Advanced Drug Delivery Reviews*, 2003, **55**, 199–215.

30   H. C. Ishikawa-Ankerhold, R. Ankerhold, and G. P. C. Drummen, *Molecules*, 2012, **17**, 4047–4132.

31   S. Padilla-Parra and M. Tramier, *Bioessays*, 2012, **34**, 369–376.

32   A. Zeug, A. Woehler, E. Neher, and E. G. Ponimaskin, *Biophysical Journal*, 2012, **103**, 1821–1827.

33   Y. Sun, H. Wallrabe, S.-A. Seo, and A. Periasamy, *Chem phys chem*, 2011, **12**, 462–474.

34   E. A. Jares-Erijman and T. M. Jovin, *Current Opinion in Chemical Biology*, 2006, **10**, 409–416.

35   H. Härmä, T. Soukka, A. Shavel, N. Gaponik, and H. Weller, *Anal. Chim. Acta*, 2007, **604**, 177–183.

36   T. Kokko, L. Kokko, T. Soukka, and T. Lövgren, *Anal. Chim. Acta*, 2007, **585**, 120–125.

37   Z. Yu, T. Kabashima, C. Tang, T. Shibata, K. Kitazato, N. Kobayashi, M. K. Lee, and M. Kai, *Analytical Biochemistry*, 2010, **397**, 197–201.

38   A. Dietrich, V. Buschmann, C. Müller, and M. Sauer, *Reviews in Molecular Biotechnology*, 2002, **82**, 211–231.

39   L. Wang and W. Tan, *Nano Lett.*, 2006, **6**, 84–88.

40   M. Köhnke, S. Schmitt, N. Ariotti, A. M. Piggott, R. G. Parton, E. Lacey, R. J. Capon, K. Alexandrov, and D. Abankwa, *Chem. Biol.*, 2012, **19**, 866–874.

41   M. Crouthamel, D. Abankwa, L. Zhang, C. DiLizio, D. R. Manning, J. F. Hancock, and P. B. Wedegaertner, *Mol. Pharmacol.*, 2010, **78**, 767–777.

42   A. K. Najumudeen, M. Köhnke, M. Šolman, K. Alexandrov, and D. Abankwa, *PLoS ONE*, 2013, **8**, e66425.

43　A. M. Sykes, N. Palstra, D. Abankwa, J. M. Hill, S. Skeldal, D. Matusica, P. Venkatraman, J. F. Hancock, and E. J. Coulson, *J. Biol. Chem.*, 2012, **287**, 43810–43824.

44　R. Liu, D. Ren, Y. Liu, Y. Deng, B. Sun, Q. Zhang, and X. Guo, *Mol Imaging Biol*, 2011, **13**, 424–431.

45　C.-Y. Zhang, H.-C. Yeh, M. T. Kuroki, and T.-H. Wang, *Nature Materials*, 2005, **4**, 826–831.

46　A. Miyawaki, J. Llopis, R. Heim, J. M. McCaffery, J. A. Adams, M. Ikura, and R. Y. Tsien, *Nature*, 1997, **388**, 882–887.

47　S. Zadran, S. Standley, K. Wong, E. Otiniano, A. Amighi, and M. Baudry, *Appl Microbiol Biotechnol*, 2012, **96**, 895–902.

48　J. Yang, H. Chen, I. R. Vlahov, J.-X. Cheng, and P. S. Low, *Proceedings of the National Academy of Sciences*, 2006, **103**, 13872–13877.

49　M. Funovics, R. Weissleder, and C.-H. Tung, *Anal Bioanal Chem*, 2003, **377**, 956–963.

50　J. M. Rosenholm, J. Zhang, W. Sun, and H. Gu, *Microporous and Mesoporous Materials*, 2011, **145**, 14–20.

51　P. I. Ravikovitch, G. L. Haller, and A. V. Neimark, *Advances in Colloid and Interface Science*, 1998, **76–77**, 203–226.

52　P. I. Ravikovitch and A. V. Neimark, *J. Phys. Chem. B*, 2001, **105**, 6817–6823.

53　D. Zhao, Q. Huo, J. Feng, B. F. Chmelka, and G. D. Stucky, *J. Am. Chem. Soc.*, 1998, **120**, 6024–6036.

54　K. S. W. Sing, *Pure and Applied Chemistry*, 1985, **57**, 603–619.

55　S. S. Vogel, C. Thaler, and S. V. Koushik, *Sci. STKE*, 2006, 331.

56　C. Berney and G. Danuser, *Biophys. J.*, 2003, **84**, 3992–4010.

57　H. Takakusa, K. Kikuchi, Y. Urano, T. Higuchi, and T. Nagano, *Anal. Chem.*, 2001, **73**, 939–942.

58　Kawanishi, Kikuchi, Takakusa, Mizukami, Urano, Higuchi, and Nagano, *Angew. Chem. Int. Ed. Engl.*, 2000, **39**, 3438–3440.

59　L. Bergman, J. Rosenholm, A.-B. Öst, A. Duchanoy, P. Kankaanpää, J. Heino, and M. Lindén, *J. Nanomaterials*, 2008, **51**, 1–9.

60　K. Chen, J. Zhang, and H. Gu, *J. Mater. Chem.*, 2012, **22**, 22005–22012.

61　W. Stöber, A. Fink, and E. Bohn, *Journal of Colloid and Interface Science*, 1968, **26**, 62–69.

62　J. Carlsson, H. Drevin, and R. Axén, *Biochem J*, 1978, **173**, 723–737.

63　J. Schindelin, I. Arganda-Carreras, E. Frise, V. Kaynig, M. Longair, T. Pietzsch, S. Preibisch, C. Rueden, S. Saalfeld, B. Schmid, J.-Y. Tinevez, D. J. White, V. Hartenstein, K. Eliceiri, P. Tomancak, and A. Cardona, *Nat. Methods*, 2012, **9**, 676–682.
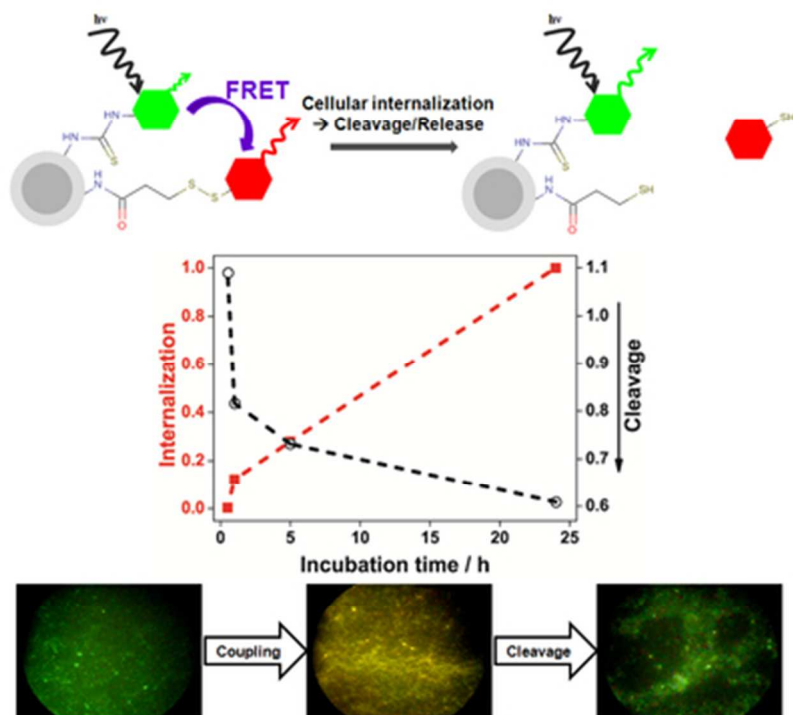
FRET-reporter particles for redox-induced release of active compounds in cells were developed. This particle system allowed following the intracellular cleavage of delivered compounds after particle internalization.
34x30mm (300 x 300 DPI)